

Modal identification of Canton Tower under uncertain environmental conditions

Xijun Ye¹, Quansheng Yan^{*1,2}, Weifeng Wang¹ and Xiaolin Yu¹

¹School of Civil Engineering and Transportation, South China University of Technology, Guangzhou 510640, China

²State Key Laboratory of Subtropical Building Science, South China University of Technology, Guangzhou 510640, China

(Received November 8, 2011, Revised February 21, 2012, Accepted April 10, 2012)

Abstract. The instrumented Canton Tower is a 610 m high-rise structure, which has been considered as a benchmark problem for structural health monitoring (SHM) research. In this paper, an improved automatic modal identification method is presented based on a natural excitation technique in conjunction with the eigensystem realization algorithm (NExT/ERA). In the proposed modal identification method, damping ratio, consistent mode indicator from observability matrices (CMI_O) and modal amplitude coherence (MAC) are used as criteria to distinguish the physically true modes from spurious modes. Enhanced frequency domain decomposition (EFDD), the data-driven stochastic subspace identification method (SSI-DATA) and the proposed method are respectively applied to extract the modal parameters of the Canton Tower under different environmental conditions. Results of modal parameter identification based on output-only measurements are presented and discussed. User-selected parameters used in those methods are suggested and discussed. Furthermore, the effect of environmental conditions on the dynamic characteristics of Canton tower is investigated.

Keywords: high-rise structure; modal identification; ambient excitation; environmental condition

1. Introduction

Output-only modal identification is a procedure by which the modal parameters of a structure can be evaluated from output-only measurements. The main advantage of this procedure is that the input force on the structures needs not to be measured. Output-only modal identification methods can be classified into two main groups, namely (1) frequency domain methods and (2) time domain methods. The major frequency domain methods, such as the peak picking method, the frequency domain decomposition technique (FDD) (Brincker *et al.* 2000) and the enhanced FDD (EFDD) technique (Brincker *et al.* 2001), are developed based on response auto/cross-spectral densities. The time domain output-only modal identification methods can be subdivided into two categories, namely (i) two-stage methods and (ii) one-stage methods. In two-stage approaches, the free vibration response estimates, including random decrement functions and response correlation functions, are obtained in the first stage from response measurements, and then modal parameters

*Corresponding author, Dr., E-mail: cvqshyan@scut.edu.cn

are identified in the second stage using any classical system identification algorithm based on impulse/free response function estimates. These classical system identification algorithms include the Ibrahim time domain method (Ibrahim *et al.* 1977), the least-squares complex exponential method (Brown *et al.* 1979), the polyreference complex exponential method (Vold *et al.* 1982), and the eigensystem realization algorithm (ERA) (Juang *et al.* 1985). In contrast to two-stage approaches, the one-stage system identification methods, such as the data-driven stochastic subspace identification (SSI-DATA) method (Van Overschee *et al.* 1996), were developed to identify modal parameters based on output-only measurements directly.

However, varying environmental conditions such as temperature, wind speed, and humidity, etc. may cause changes in modal parameters. In previous studies, variations in modal parameters due to changes in environmental conditions have been shown to be significant; they may even be larger than those caused by structural damage (Abdel Wahab *et al.* 1997, Peeters *et al.* 2001, Xia *et al.* 2006, He *et al.* 2007, Zhou *et al.* 2011a,b). Therefore, in order to develop a robust and reliable vibration-based SHM system, it is of great importance to study the correlation between the modal parameters identified and the varying environmental conditions.

The Canton Tower in Guangzhou, China, is a high-rise structure with a height of 610 m, which has been considered as a benchmark problem for SHM research. In this benchmark study, a set of field monitoring data including acceleration, wind direction, wind speed and ambient temperature covering a period of 24 hours and a reduced-order finite element (FE) model of the Canton Tower have been provided (Ni *et al.* 2012), which can be directly used for output-only modal identification and FE model updating.

In this study, three output-only modal identification algorithms are applied to the ambient vibration measurement data acquired from the Canton Tower. They are: (1) EFDD, a nonparametric frequency domain system identification method, which is a sophisticated extension of the well-known peak picking technique; (2) SSI-DATA, a one-stage approach, which directly works with the measured time histories; (3) an improved automatic modal identification method based on NExT-ERA, which is a two-stage modal identification technique. Finally, the changes in natural frequencies and damping ratios under different environmental conditions are investigated.

2. Output-only modal identification methods

2.1 Frequency domain decomposition

The basic principle of the frequency domain decomposition (FDD) method was described by Prevosto (1982) and Corrêa and Costa (1992). The method was, however, better detailed and systematized by Brincker *et al.* (2000), with the objective of overcoming the limitation of the Peak-Picking method related to the separation of closely spaced modes. It was subsequently enhanced in estimating modal damping ratios (Brincker *et al.* 2001).

The FDD method approximately decomposes the spectral density matrix into a set of single degree of freedom (DOF) systems using singular value decomposition (SVD), allowing close modes to be identified with high accuracy. In this method, the relationship between output responses $y(t)$ and unknown inputs $x(t)$ can be expressed as

$$G_{yy}(j\omega) = H^*(j\omega)G_{xx}(j\omega)H(j\omega)^T \quad (1)$$

where $G_{yy}(j\omega)_{m \times m}$ is the power spectral density (PSD) matrix of the responses; $G_{xx}(j\omega)_{l \times l}$ is the matrix of the input; $H^*(j\omega)$ is the complex conjugate of the $(m \times 1)$ FRF matrix; $H(j\omega)^T$ is the transpose of the $(m \times 1)$ FRF matrix; and m is the number of output DOFs.

In the FDD method, the first step is to obtain an estimate of the output PSD matrix, $\hat{G}_{yy}(j\omega)$, for each discrete frequency $\omega = \omega_i$. This can be done by creating an array of FRFs using FFT information from each DOF in a system

$$\hat{G}_{yy}(j\omega) = \{F_y(j\omega)_i\} * \{F_y^*(j\omega)_i\}^T \quad (2)$$

where $\{F_y(j\omega)_i\}$ = array of FFT values for a specific DOF at a given frequency ω_i and $\{F_y^*(j\omega)_i\}^T$ = the complex conjugate transpose (Hermitian matrix) of that array (Allemang 1999).

The second step is to extract singular values and singular vectors from the PSD of the response by taking the SVD of the matrix $\hat{G}_{yy}(j\omega)$

$$\hat{G}_{yy}(j\omega) = U_i S_i U_i^H \quad (3)$$

where the matrix $U_i = [u_{i1}, u_{i2}, \dots, u_{im}]$ is unitary matrix holding singular vectors u_{ij} ; S_i is diagonal matrix holding the scalar singular values S_{ij} ; and U_i^H is Hermitian matrix of U_i . Near a peak in the PSD function for a given mode, this mode or a possible close mode will be dominant. Thus, the first singular vector, u_{i1} , can be an estimate of the mode shape ϕ_i : $\phi_i = u_{ij}$.

An extension of the FDD method that allows for the detection of additional modal information (modal frequencies and damping ratios) is often called enhanced frequency domain decomposition (EFDD) (Brincker *et al.* 2001).

In the EFDD method, the natural frequency and damping ratio of a mode are identified from the related SDOF CSD function. Therefore, the SDOF CSD function is fed back to the time domain by inverse Fourier transformation, and the frequency and damping ratio of the mode concerned are estimated from the zero-crossing times and the logarithmic decrement, respectively, of the corresponding SDOF autocorrelation function.

2.2 Data-driven stochastic subspace identification

Unlike the two-stage methods, the data-driven stochastic subspace identification method works directly with the recorded time domain signals. A general overview of subspace identification is provided by Van Overschee and De Moor (1996). The method assumes that the dynamic behavior of a structure excited by white noise can be described by a stochastic state space model:

$$\begin{aligned} x_{k+1} &= Ax_k + w_k \\ y_k &= Cx_k + v_k \end{aligned} \quad (4)$$

where $x_k \in R^{2n_p \times 1}$ is the internal state vector; n_p is the number of poles; $y_k \in R^{l \times 1}$ is the measurement vector; w_k, v_k are white noise terms representing the process noise and measurement noise together with the unknown inputs; $A \in R^{2n_p \times 2n_p}$ is the state matrix containing the dynamics of the system; and $C \in R^{l \times 2n_p}$ is the output matrix, translating the internal state of the system into observations.

The subspace method then identifies the state space matrices based on the measurements and by use of robust numerical techniques such as QR-factorization, SVD and least squares. Roughly, the QR results in significant data reduction, whereas SVD is used to reject the noise assumed to be

represented by the higher singular values. Once the mathematical description of the structure, i.e., the state space model is found, it is straightforward to determine the modal parameters by eigenvalue decomposition: natural frequencies, damping ratios and mode shapes.

Several variants of stochastic subspace identification exist. They differ in the weighting of the data matrices before application of SVD. There are three main algorithms for weighting matrices: the Unweighted Principal Component (UPC) algorithm, the Principal Component (PC) algorithm and the Canonical Variate Analysis (CVA) algorithm. In the present study, SSI-DATA associated with CVA is applied.

2.3 Eigensystem Realization Algorithm (ERA)

The Eigensystem Realization Algorithm (ERA) is a multi input-multi output (MIMO) time domain modal identification technique, and has been widely used in the field of civil engineering (Juang *et al.* 1985).

In ERA, the Hankel matrix is formed as

$$H(k-1) = \begin{bmatrix} h(k) & h(k+1) & \dots & h(k+s) \\ h(k+1) & h(k+2) & \dots & h(k+s+1) \\ \vdots & \vdots & \ddots & \vdots \\ h(k+r) & h(k+r+1) & \dots & h(k+r+s) \end{bmatrix} \quad (5)$$

where $h(k)$ = response vector at the k -th time step. The parameters s and r correspond to the number of columns and rows of the response vectors in the matrix.

The Hankel matrix is evaluated for $\mathbf{H}(\mathbf{0})$ and a singular value decomposition is performed as

$$H(\mathbf{0}) = R\Sigma S^T \quad (6)$$

where R and S^T are the matrices of the left and right eigenvectors of $\mathbf{H}(\mathbf{0})$, respectively; and Σ is a diagonal matrix of singular values. Relatively small singular values along the diagonal of Σ correspond to computational (nonphysical) or noise modes. The rows and columns associated with the computational modes are eliminated to form the condensed version Σ_n , R_n and S_n of these matrices. The estimates of the state-space matrices for the discrete-time structural model are found using

$$\begin{aligned} \hat{A} &= \Sigma_n^{-1/2} R_n^T H(\mathbf{1}) S_n \Sigma_n^{-1/2} \\ \hat{B} &= \Sigma_n^{-1/2} S_n^T E_r \\ \hat{C} &= E_m^T R_n \Sigma_n^{-1/2} \end{aligned} \quad (7)$$

where R_n and S_n are formed by eliminating columns of R and S , i.e., the left and right eigenvectors of the Hankel Matrix $\mathbf{H}(\mathbf{0})$ corresponding to relatively small or negligible singular values. It is noted that $R_n^T R_n = I$ and $S_n^T S_n = I$. $\mathbf{H}(\mathbf{1})$ is a time-shifted Hankel matrix of $\mathbf{H}(\mathbf{0})$. $E_m^T = [I \ 0]$ and $E_r^T = [I \ 0]$ are used for selecting the system matrices \hat{B} and \hat{C} from extended controllability and observability matrices.

The estimated discrete-time realization then needs to be transformed into the continuous-time domain format. Let us consider the eigenvalue problem for \hat{A}

$$\hat{A} = \hat{\psi} \hat{\Lambda} \hat{\psi}^{-1} \quad (8)$$

where $\hat{\Lambda}$ and $\hat{\psi}$ = eigenvalue and eigenvector matrices, respectively. The natural frequencies, ω_i , damping ratios, ζ_i , and the mode shapes, ϕ_i , of the continuous-time structural model can be found as follows:

$$\omega_i = \sqrt{\bar{\sigma}_i^2 + \bar{\Omega}_i^2}, \quad \zeta_i = -\cos[\tan^{-1}(\bar{\Omega}_i/\bar{\sigma}_i)], \quad \hat{\phi}_i = \hat{C} \hat{\psi}_i \quad (9)$$

where $\hat{\Lambda} = \text{diag}(\bar{\sigma}_i + j\bar{\Omega}_i)$, $\bar{\sigma}_i + j\bar{\Omega}_i = \ln(\bar{\sigma}_i)/\Delta t \pm \ln(\bar{\Omega}_i)/\Delta t$, Δt = sampling period of data records.

2.4 Natural Excitation Technique (NExT)

NExT was developed by James *et al.* (1993), who demonstrated that when a system is excited by stationary white noise, the cross-correlation function $R_{ij}(\tau)$ between two stationary response signals $x_i(t)$ and $x_j(t)$ can be shown as Eq. (9)

$$R_{ij}(\tau) = \sum_{r=1}^n \frac{\phi_{ir} A_{jr}}{m_r \omega_{dr}} \exp(-\zeta_r \omega_r \tau) \sin(\omega_{dr} \tau + \theta_r) \quad (10)$$

where ϕ_{ir} is the i -th component of the r -th mode shape; A_{jr} is a constant; and m_r is the r -th modal mass. The above result shows that $R_{ij}(\tau)$ in Eq. (10) is a sum of complex exponential functions (modal responses), which is of the same mathematical form as the free vibration decay or the impulse response of the original system. Thus, the cross-correlation functions evaluated from response data can be used as free vibration decay or as impulse response in time-domain modal extraction schemes to avoid measurement of white noise inputs. The term $\phi_{ir} A_{jr}$ in Eq. (10) is identified as a mode-shape component. In order to eliminate the A_{jr} term and retain the true mode-shape component ϕ_{ir} , all measured channels are correlated against a common reference channel, say x_j . Then, identified components all possess the common A_{jr} component, which can be normalized to obtain the desired mode shape ϕ_{ir} .

In most experimental modal testing or field ambient vibration testing, the number of input points is less than that of the output points. In particular, the ERA combined with the NExT technique frequently assumes a limited number of reference nodes. For example, one reference node is normally selected for the calculation of the impulse response function in the form of cross-correlation functions. Thus temporal consistency of the identified properties in the form of the modal participation factors is highly dependent on the choice of reference nodes, since the reference node might have relatively less degree to which some of the modes participate in the response than others. Thus, for effective implementation, the reference point should be selected to be a response that is not located at any modal node.

Previous experiences have shown that one cannot rely on a single reference DOF to identify all modes (He *et al.* 2007, Nayeri *et al.* 2009). The optimum accuracy for the identification of different modes typically occurs at different choices of the reference DOFs. In the following, we formulate the identification algorithm by using multiple DOFs as the reference points.

3. Improved automatic modal identification method

3.1 Mode accuracy indicator

In practical implementation, ERA analysis can contain a significant number of computational (nonphysical) modes due to nonlinearity, noise effects, inadequate excitations, etc. In order to distinguish the physical modes from spurious modes, several consistency indicators are introduced to distinguish the nonphysical modes from modal characteristics identified through ERA analysis.

An autonomous modal identification technique was suggested using the Consistent Mode Indicator (CMI) as a primary metric in ERA analysis (Pappa *et al.* 1993, 1998). In this approach, physical modes are filtered based on the CMI values. It is followed by a logical rule-based engine to judge whether the modes found in next iterations are new or existing modes and to choose the best estimation among the same modes. The CMI is calculated as a product of Extended Modal Amplitude Coherence (EMAC) and Modal Phase Collinearity (MPC). EMAC is calculated as a product of output (observability) and input (controllability) EMAC values. These indicators have been successfully used in the previous studies with reliable verifications. Modes with 0% CMI values indicate spurious modes. Even though a 50% CMI cut-off value is routinely used in practice, it allows some real modes with poor accuracy to be deleted because another ERA analysis can identify the modes (Pappa 1999). Thus a wide range of CMI values still poses considerable difficulties and requires close interaction with experienced experts.

An improved consistency indicator called CMI from the observability matrix (CMI_O) is suggested by Yun (2009), who demonstrated that CMI_O is also consistent under high damping ratios.

$$CMI_O_i = \left\{ \frac{1}{q} \sum_{j=1}^q EMAC_{ij}^O \right\} \times MPC_i \times 100(\%) \quad (11)$$

where MPC is the modal phase collinearity from Reference; $EMAC_{ij}^O$ is EMAC from the observability matrix; i indicates the i -th mode; j indicates the j -th output point; and q indicates the total number of output points, i.e., sensor locations. The temporal consistency in the form of observability (or mode shapes) shows a reliable measure of a degree to which the identified modes participate in the response since they are calculated for every measurement point. Thus in the improved indicator, only output-based EMAC values are taken into account.

3.2 Improved stabilization diagram method

The stabilization diagram is widely used as a robust tool to distinguish the physical modes from spurious modes. In the traditional stabilization diagram method, the stabilization procedure performs

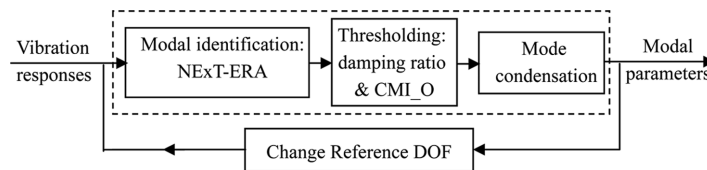


Fig. 1 Three steps of the multiple reference DOFs stabilization diagram method

sequentially for all system orders up to a user-specified maximum. At each step, the modes identified at the current system order are compared with those identified at the previous system order, the criteria used are (Peeters 2001)

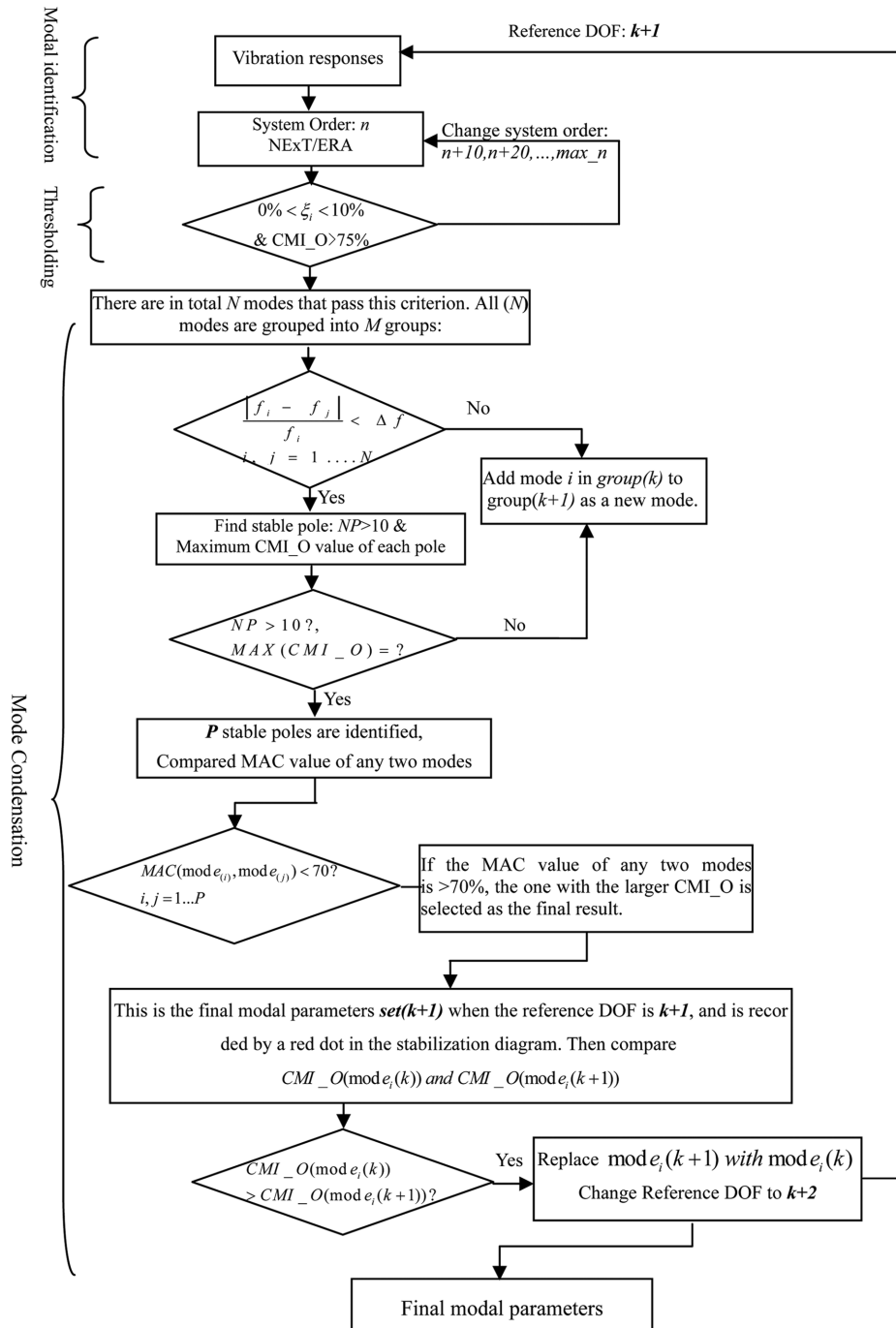


Fig. 2 Flowchart of the proposed algorithm

- (1) Criterion (stable frequencies): $\delta f = (f_n - f_{n-1}) / f_{n-1} \times 100\%$
- (2) Criterion (stable damping ratios): $\delta \xi = (\xi_n - \xi_{n-1}) / \xi_{n-1} \times 100\%$
- (3) Criterion (stable mode shapes): $MAC_{n,n-1} > 95\%$

where δf is the relative frequency difference; $\delta \xi$ is the relative damping ratio difference; and MAC is the MAC value between two modes.

In the present study, an improved multiple reference DOFs stabilization diagram method based on ERA is introduced. CMI_O is used as the criteria and set as 75%. The algorithm consists of three main steps as shown in Fig. 1.

Fig. 2 illustrates the flowchart of the proposed algorithm. There are two main iteration loops: the outer loop changes the reference DOF, while the inner loop changes the model order for each reference DOF. The iteration loops are detailed as follows.

(1) NExT-ERA is implemented to identify modal parameters when the reference DOF is set to k . By setting different system orders, modal parameters of different system orders are identified. For each system order, the damping ratio and CMI_O value are used as criterion. If the modal damping ratio and CMI_O value of a particular mode identified is less than 10% and greater than 75%, respectively ($0\% < \xi < 10\%$ & $CMI_O > 75\%$), it would move to the next procedure and be plotted on the diagram, or it will be eliminated as a spurious mode. There are in total N modes that pass this criterion.

(2) Mode condensation is performed. If the relative frequency difference of any two modes is less than Δf ($\delta f = (f_i - f_j) / f_i \times 100\% < \Delta f$), they are considered the same mode and recorded as temporary stable modes. Thus all N modes are grouped into M poles.

(3) Only poles that are more than NP times stable are selected as stable poles to exclude accidentally stable poles, and the representative of a column of stable poles at a certain frequency is the one with maximum CMI_O value. Thus P stable poles are identified.

(4) Compare MAC value of any two modes within P stable poles. Make sure that the MAC values of any two retained representative modes are less than 70%. And then the identified modal parameters set (k) are recorded by a red dot on the stabilization diagram.

(5) The algorithm is implemented when the reference DOF is changed to $k+1$, and the modal parameters set ($k+1$) can be obtained. Then CMI_O value of the two sets of parameters ($set(k)$ and $set(k+1)$) are compared to get $newest(k+1)$. In brief, the mode with the greater CMI_O value is considered more accurate. Finally, all DOFs have been set as reference DOF, and final modal parameters can be obtained.

4. Description of the measurement of canton tower

A set of ambient vibration, temperature, wind speed and wind direction measurement data is extracted from the SHM system deployed installed on the Canton Tower (Ni *et al.* 2009a). The data used were recorded from 18:00 pm on 19 January 2010 to 18:00 pm on 20 January 2010, for a period of 24 hours.

The accelerometer positions and measurement directions are shown in Fig. 3. A total of 20 uni-axial accelerometers were installed at eight levels. The 4th level and the 8th level were equipped with four uni-axial accelerometers, two for measurement of the horizontal acceleration along the

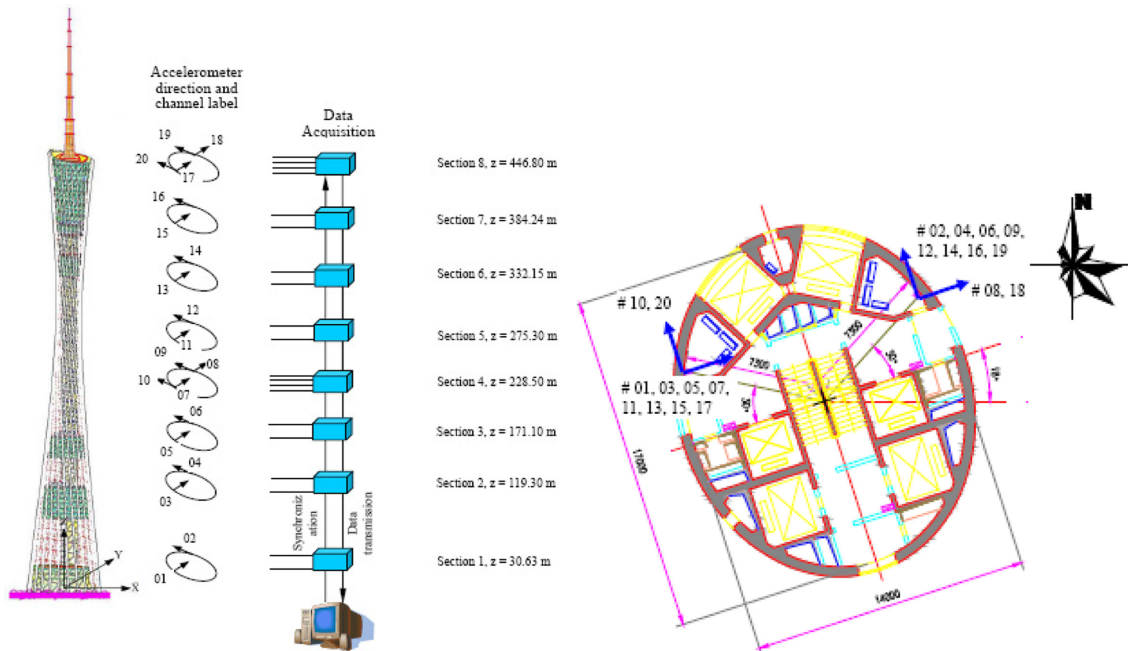


Fig. 3 (a) Position of the accelerometers and data acquisition system and (b) measurement directions of acceleration and channel labels

long-axis of the structure, and the other two for the short-axis. At the other six levels, each section was equipped with two uni-axial accelerometers, one along the long-axis and the other along the short-axis. In addition, an anemometer and thermocouple were installed at the top of the main tower where the altitude is 461.1 m. The sampling frequency of the acceleration and wind data was set to 50 Hz. The temperature data were measured every minute (Ni *et al.* 2012).

5. Modal analysis of canton tower

The temperature, wind speed and wind direction data measured during the 24 hours are represented in Fig. 4. In order to further investigate how the modal parameters change when

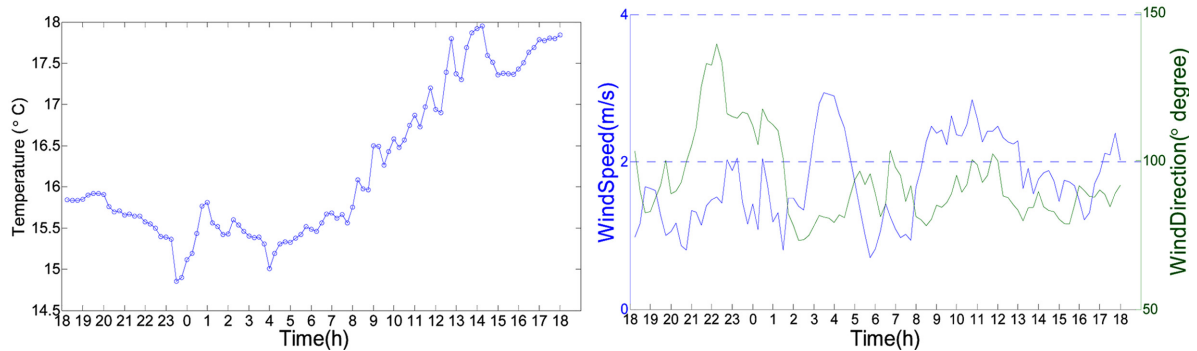


Fig. 4 (a) Temperature data and (b) wind speed and wind direction data

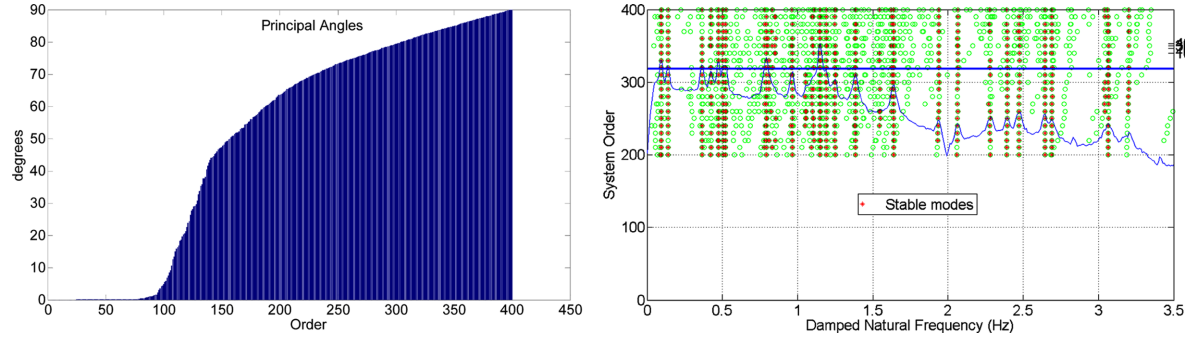


Fig. 5 Analysis results for the measurement data for the period 12:00 to 13:00 (the first 15 minutes): (a) principle angles and (b) stabilization diagram

subjected to different environmental effects, the acceleration data of every hour was divided into four sets, and each set of data lasts for 15 minutes and has 45,000 samples. There are totally 96 sets of data.

Prior to modal identification, signal pre-processing including detrending and band-pass filtering should be conducted. Since the frequency range of interest is less than 5 Hz, the data is band pass filtered with a 5-th order band-pass Butterworth filter in the range 0.05-2 Hz after detrending. Then the data after pre-processing is down sampled to 10 Hz. In the present study, the first 12 modes are investigated.

5.1 Implementation of SSI-Data

The implementation of the SSI-Data algorithm only requires two parameters to set up, i.e., the dimensions of the Hankel matrices used in the orthogonal projections, and the model order used to truncate the singular value decompositions.

Hankel matrices have a dimension of $2i$ block rows by j columns. The number of block rows (i) is a user-defined index which is large enough, i.e., it should at least be larger than the maximum order (n) of the system to be identified. The number of columns (j) is typically equal to $s-2i+1$, which implies that all given data samples (s) are used. Thus, a suggestion was given by Van Overschee and De Moor (1996) that $i = \text{maximum order}/\text{number of outputs}$. In this study, this suggestion is used to determine the block row of the Hankel matrix; thus the number of columns (j) is equal to $s-2i+1$.

The system order of the identified model, using the Canonical Variate Algorithm (CVA), is determined by the number of principal angles between the row spaces of the past and the future outputs that are different from 90 degrees. However, working with real data, these principle angles never completely reach 90 degrees. An example of principle angles and a stabilization diagram, calculated for a sample 15 minutes record is shown in Fig. 5. It is seen from Fig. 5(a), most of the principle angles fail to reach 70 degree for the system order (n) < 200. Therefore, n_{min} should be chosen to be larger than 200 and n_{max} could be arbitrarily chosen. A stabilization diagram identifying frequencies vs. system orders is shown in Fig. 5(b). By choosing the criterion $\delta f = 3\%$, $\delta \xi = 40\%$ and $MAC_{n,n-1} = 95\%$, it takes approximately 20 minutes to finish the modal identification in the system order range of [200, 400].

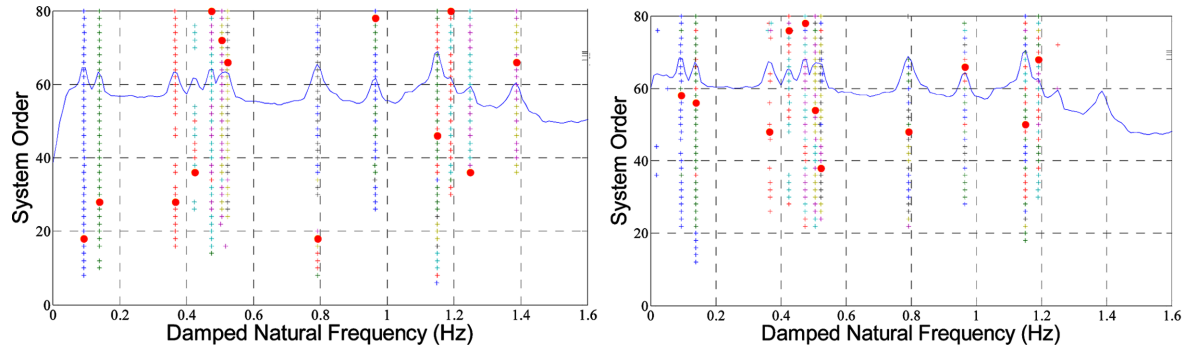


Fig. 6 Analysis results for the measurement data for the period 12:00 to 13:00 (the first 15 minutes), (Stabilization Diagram by NExT-ERA: (a) Ref. DOF: Channel 18# and (b) Ref. DOF: Channel 19#)

5.2 Implementation of automatic modal identification based on NExT-ERA

For NExT, the correlation function can be estimated by the inverse Fourier transform of the cross power spectral density (CPSD), where the CPSD is computed directly from the data. There are some algorithmic parameters that must be selected based on the user's judgment. The window size required for the computation of the CPSD is one of those parameters. In a previous study on the finite-element model of the IASC-ASCE benchmark problem, Caicedo *et al.* (2004) concluded that the NExT-ERA results are not sensitive to the window size used in the computation of the CPSD. Thus, in the present study, Hanning window is implemented with its size and overlap set to be 4096 and 50%, respectively.

Another important user-selectable parameter is the dimensions of the Hankel matrix. Juang and Pappa (1985) suggested using a Hankel matrix whose number of columns is 20 times the number of frequencies, and whose number of rows is 2-3 times the number of columns. Another commonly used practice to select these dimensions is associated with the quality of the free responses. Under this criterion, the Hankel matrix is built making full use of the decaying signal, provided that the signal-to-noise ratio is high.

For each set of data, as shown in Fig. 6, on each loop one channel is chosen as the reference channel, the dimensions of the Hankel matrix is set to 800×400 ((400 block columns for one input (one reference channel); 40 block rows with either 20 rows in each block (20 output channels)). The system order is set to be from 2 to 80, with a step increase of 2. It takes approximately 5 minutes to finish the identification of one set of data.

Two stabilization diagrams based on different reference DOFs are shown in Fig. 6. Making use of different reference DOFs, different numbers of modes are identified. Both diagrams show that the dynamic behavior of the structure is well represented by state-space models of the order between 40 and 80. A system order under 30 is high enough to identify lower vibration modes, while for higher vibration modes a relatively high system order is needed. There are two groups of closely spaced modes, i.e., $f = 0.4239, 0.4748, 0.5055, 0.5225$ Hz and $f = 1.1504, 1.1910, 1.2507$ Hz. Since the relative frequency (and node shape) difference between the two closely spaced modes is tiny and highly correlated, the criteria used for selecting stable poles should be specified to the values which can effectively distinguish physical modes from spurious modes.

It is well known that damping ratios of civil engineering structures under ambient excitation are

usually less than 5%. But as reported in previous studies, it is difficult to achieve reliable estimates of the damping ratios, which are not only justified by the uncertainties of the method but also by the variation in damping with the levels of oscillation associated with the wind speed. Thus the damping ratio criterion is set to be $0\% < \xi < 10\%$. Yun (2009) indicated that modes with CMI_O values greater than approximately 85% can be identified with high confidence. CMI_O=75% is selected in the present study; it allows some real modes with poor accuracy which may be caused by weak excitation, to be detected. In this case, $\delta f = 3\%$ is small enough to separate the closely spaced modes. To make sure that the poles selected are stable enough, $NP = 10$ is defined. The last step of this improved algorithm is to make sure that the MAC values of any two retained representative modes should be less than a specified value. It is worth noting that for the closely spaced modes as presented in this study, a suitable value of 70% is established after heaps of tests. However, for the modes which are not closely spaced, a smaller value of MAC should be specified. Thus, the criteria listed below can successfully identify the first 12 modes.

- (1) $0\% < \xi < 10\% \ \& \ \text{CMI_O} > 75\%$
- (2) $\delta f = (f_i - f_j) / f_i \times 100\% < 3\%$
- (3) $NP = 10$
- (4) $\text{MAC} = 70\%$

5.3 Implementation of Enhanced Frequency Domain Decomposition

In the implementation of EFDD, there are a number of parameters that have effect on the algorithm. The first is the length of the fast Fourier transform (NFFT) used in creating the cross-power spectral matrix. The NFFT determines the frequencies at which the power spectral density is calculated. Larger values of NFFT will decrease the frequency step, increasing the precision. Lower values of NFFT will provide a smoother singular value plot making peak picking easier. In this study, a NFFT value of 2^{13} is used. This value can provide a small enough frequency step, i.e., 0.0012 Hz while providing a smoother plot for ease of peak picking. The cross power spectral density also depends on the windowing function used and the amount of overlap between windows. A Hanning window with a 50% overlap is selected.

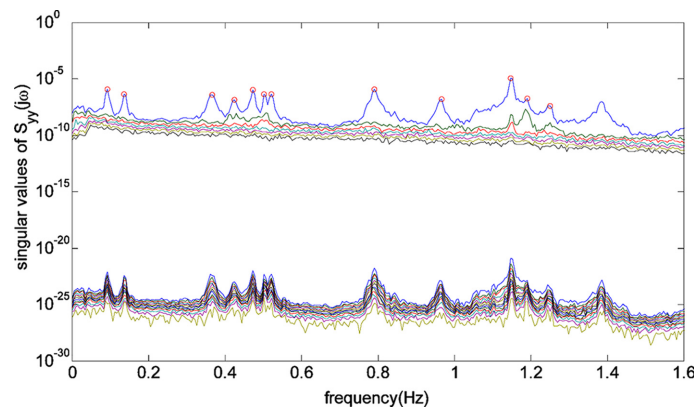


Fig. 7 Analysis results for the measurement data for the period 12:00 to 13:00 (the first 15 minutes). (singular values by EFDD)

The modal frequencies are estimated at peak locations in the singular values versus frequency plot as shown in Fig. 7, and the mode shapes are estimated by the first singular vector at the corresponding frequencies.

5.4 Results and comparison

Totally 96 sets of modal parameters including natural frequencies, damping ratios and mode shapes are obtained. The mean values of the identified modal parameters and the FEM analysis results are listed in Table 1. The results are in agreement with those presented by Faravelli *et al.* (2010) and Niu *et al.* (2011).

The 96 sets of modal parameters obtained by NExT-ERA are shown in Fig. 8. The coefficients of variation of identified natural frequencies and damping ratios from different methods are shown in Fig. 9.

Figs. 8(a) and 9(a) illustrate that the variation in the natural frequencies among the sets is very

Table 1 Mean values of identified modal parameters and FEM analysis results

Mode order	FEM	NExT-ERA			SSI-DATA		EFDD	
	Frequency: (Hz)	Frequency: (Hz)	Damping ratio: ξ (%)	CMI_O (%)	Frequency: (Hz)	Damping ratio: ξ (%)	Frequency: (Hz)	Damping ratio: ξ (%)
1	0.1103	0.0937	1.1763	99.04	0.0935	0.9583	0.0924	1.6803
2	0.1587	0.1383	0.8991	99.28	0.1386	0.6378	0.1367	1.6436
3	0.3462	0.3657	0.418	98.37	0.3659	0.5022	0.3637	1.678
4	0.3688	0.4239	0.3272	98.26	0.4238	0.2203	0.4248	0.3426
5	0.3994	0.4748	0.2165	97.66	0.4744	0.1843	0.4701	2.2864
6	0.4605	0.5055	0.3018	96.68	0.5052	0.2929	0.5029	0.4952
7	0.4849	0.5225	0.3253	97.67	0.5225	0.4366	0.5225	0.3938
8	0.738	0.7953	0.2381	95.22	0.7952	0.4519	0.791	0.5571
9	0.9025	0.965	0.2864	94.8	0.9648	0.3022	0.9652	0.4502
10	0.9971	1.1504	0.1379	92.06	1.1506	0.1379	1.1494	0.2248
11	1.0372	1.191	0.1359	96.04	1.1908	0.1712	1.1914	0.2237
12	1.1218	1.2507	0.1745	94.23	1.2504	0.2509	1.2463	0.586

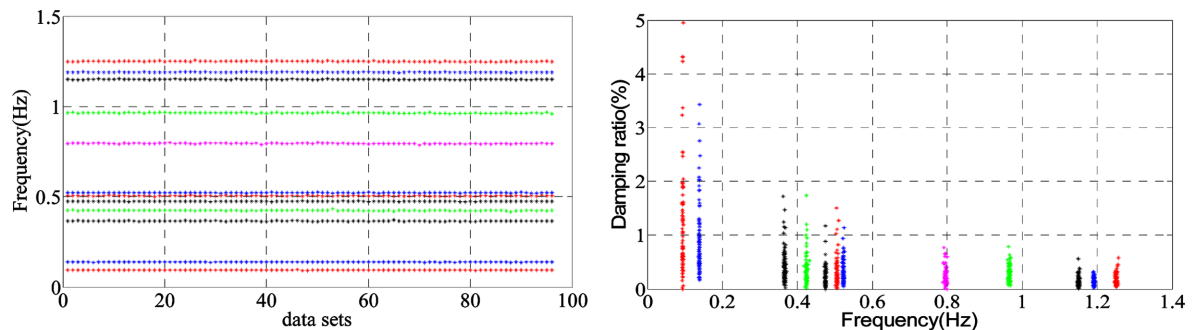


Fig. 8 Plots of 96 sets of modal parameters identified using NExT-ERA: (a) natural frequencies and (b) damping ratios

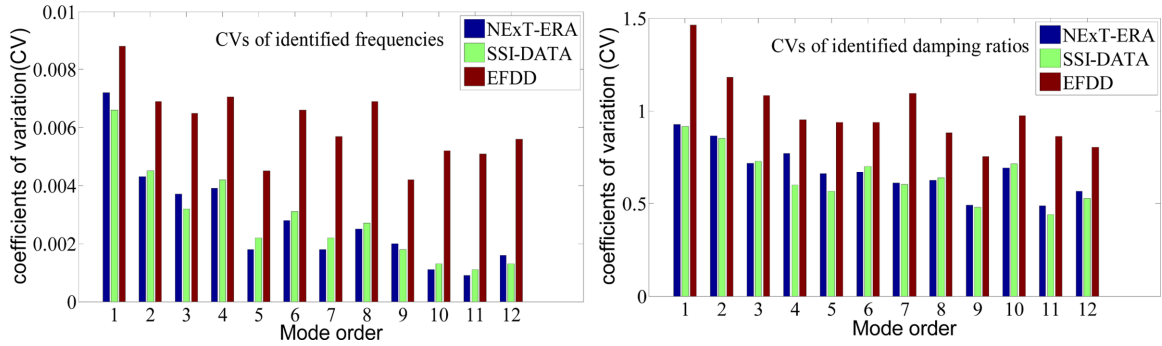


Fig. 9 Coefficients of variation of identified natural frequencies and damping ratios (a) natural frequencies and (b) damping ratios. (Note: coefficients of variation (CV) = standard deviation / mean)

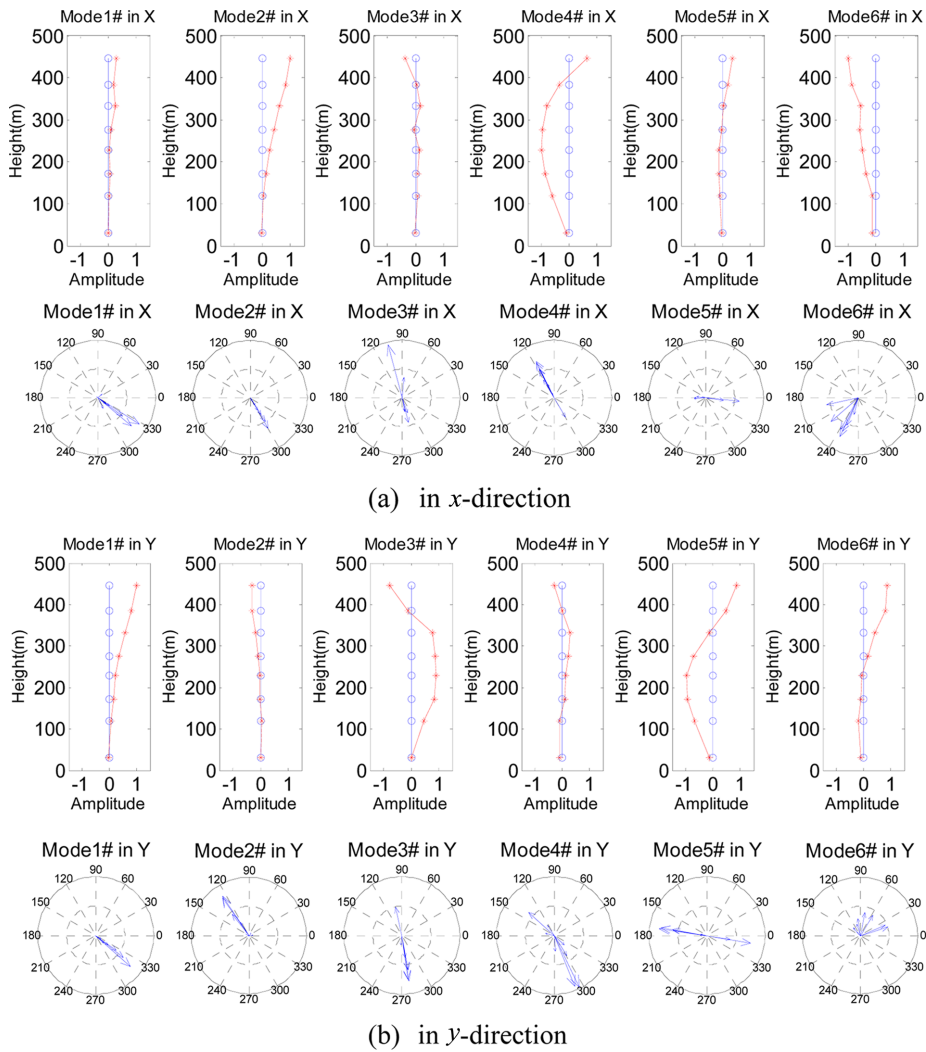


Fig. 10 Identified mode shapes of Canton Tower using NExT/ERA: 1st to 6th modes

small (the coefficients of variation between 0.0009 and 0.0072 for NExT-ERA,, the coefficients of variation between 0.0007 to 0.0048 for SSI-DATA, and the coefficients of variation between 0.0011 and 0.0126 for EFDD), whereas the damping ratios have a significant dispersion as shown in Figs. 8(a) and 9(b): the coefficients of variation between 0.4908 (mode 9) and 0.8754 (mode 1) for NExT-ERA, the coefficients of variation between 0.2957 (mode 9) and 1.5364 (mode 5) for SSI-DATA, and the coefficients of variation between 0.5611 (mode 11) and 1.0463 (mode 1) for EFDD. Furthermore, the damping ratios of the lower vibration modes are much more scattered than the higher vibration modes (Fig. 8(b)).

It is seen from Table 1 that the CMI_O values of the first 12 modes, identified using NExT-ERA,

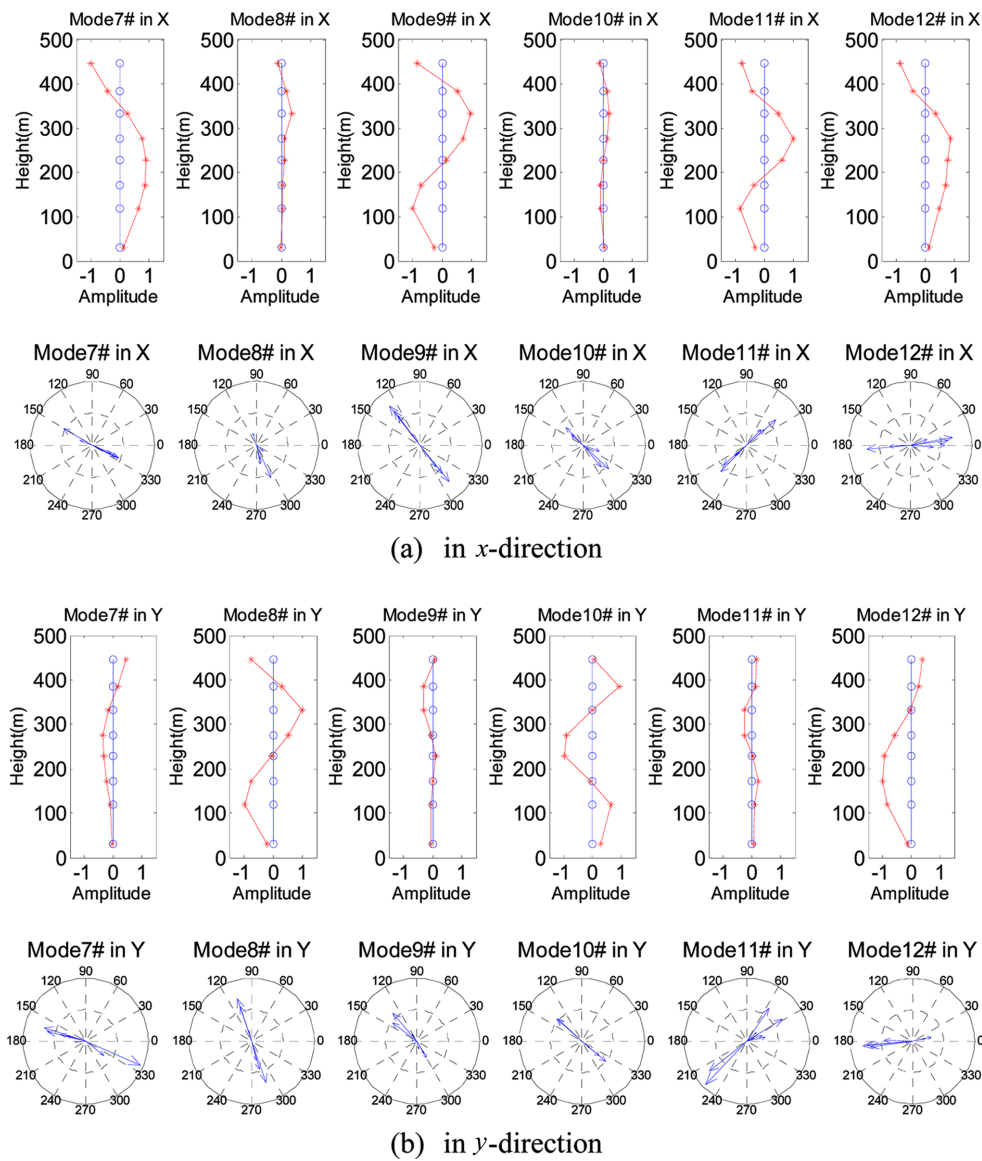


Fig. 11 Identified mode shapes of Canton Tower using NExT/ERA: 7th to 12th modes

are greater than 92%, with high confidence. It is observed that the natural frequencies identified using different methods are in excellent agreement, although they are not thoroughly consistent with the FEM results, especially for the higher vibration modes. That means the FE model needs to be updated for further study, but it is not the scope of this study. The relative difference in the identified damping ratios obtained using different methods is significantly larger than that of the corresponding identified natural frequencies, and the damping ratios estimated using EFDD are greater than those estimated using SSI-DATA and NExT-ERA. Such a phenomenon has been well reported in structural identification literature (Magalhães *et al.* 2007, He *et al.* 2009): the estimation uncertainty of damping ratios is inherently higher than that of the corresponding natural frequencies. The following facts are also worth noting regarding the identification of damping ratios: (1) for output-only modal identification methods, as the input signals do not strictly satisfy the broadband assumption behind the formulation of the output-only methods. Different methods provide modal parameter estimators with different intramethod and intermethod statistical properties (bias, variance, covariance), depending on the frequency content of the input excitation and the level of violation of the assumed amplitude stationarity; and (2) linear viscous damping is assumed in the structural model underlying the system identification, which in many cases may not characterize well the actual energy dissipation mechanisms of the structure. These are sources of modeling uncertainties that would contribute to the uncertainty of the modal damping ratio identified.

Complex model shapes are identified. Figs. 10 and 11 demonstrate the mode shapes of the Canton Tower identified using NExT-ERA. Normalization mode shapes are given at the top. Normalization was performed by using the real components of the complex mode shapes and then scaling the largest component of the real mode shape vector to unity. Also, the complex mode shapes were plotted in polar plane as shown in Fig. 10(b), where each arrow in the polar plane represents a complex component of the mode shape vector. These polar plots have the advantage of directly showing the extent of the non-proportional damping characteristics of a vibration mode. If all complex value components of a mode shape vector are collinear, i.e., in phase or 180° out of phase, this vibration mode is said to be classically (or proportionally) damped. On the other hand, the more these mode shape components are scattered in the complex plane, the more the vibration mode is nonclassically (or non-proportionally) dampened.

From Figs. 10 and 11, it is seen that most of the vibration modes identified in this study are nonclassically dampened. The Canton Tower is a tube-in-tube structure, which comprises a reinforced concrete inner tube and a steel outer tube adopting concrete-filled-tube columns (Ni *et al.* 2009a). The steel structure and the RC structure have different damping ratios, thus composing a nonclassical damping system.

6. Environmental effects

The effects of temperature variability on the measured modal properties of structures have been addressed in several studies (Abdel Wahab *et al.* 1997, Peeters *et al.* 2001, Hua *et al.* 2007, Ni *et al.* 2009b). It is intuitive that temperature variation may not only change the material properties of a structure, but also alter the boundary conditions of a system. Wind-induced vibration also plays an important role. As a high-rise structure vibrates in the wind, the energy input from the wind-induced vibration becomes larger than the energy dissipated by damping, causing fluttering or buffeting (Sohn 2007, Zhou *et al.* 2008, Chen *et al.* 2011, Xia *et al.* 2011).

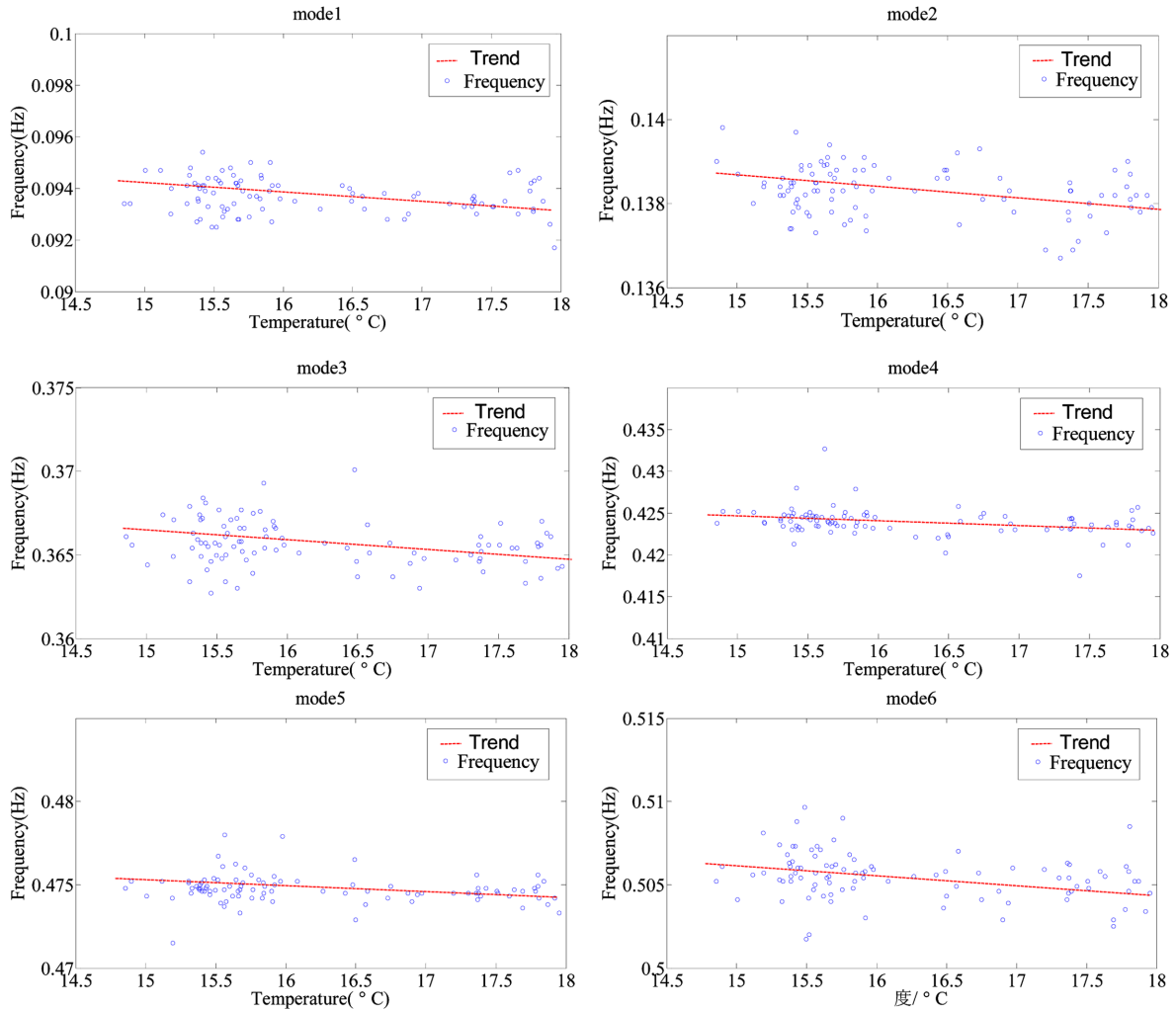


Fig. 12 Variation in natural frequencies with ambient temperature

6.1 Natural frequencies

Fig. 12 shows the changes in the first six natural frequencies with respect to the ambient temperature. In these plots, slight temperature variations were observed and the corresponding trends are shown by solid lines. Although the frequency variations are very small, the trends can be easily recognized, which indicate that natural frequencies decrease with increasing temperature.

6.2 Damping ratios

Fig. 13 shows the changes of the first six damping ratios with respect to wind speed. The data scatter is much larger than that observed in natural frequencies, which does not reach general conclusions. For different modes, the trend is different. No uniform trend is observed.

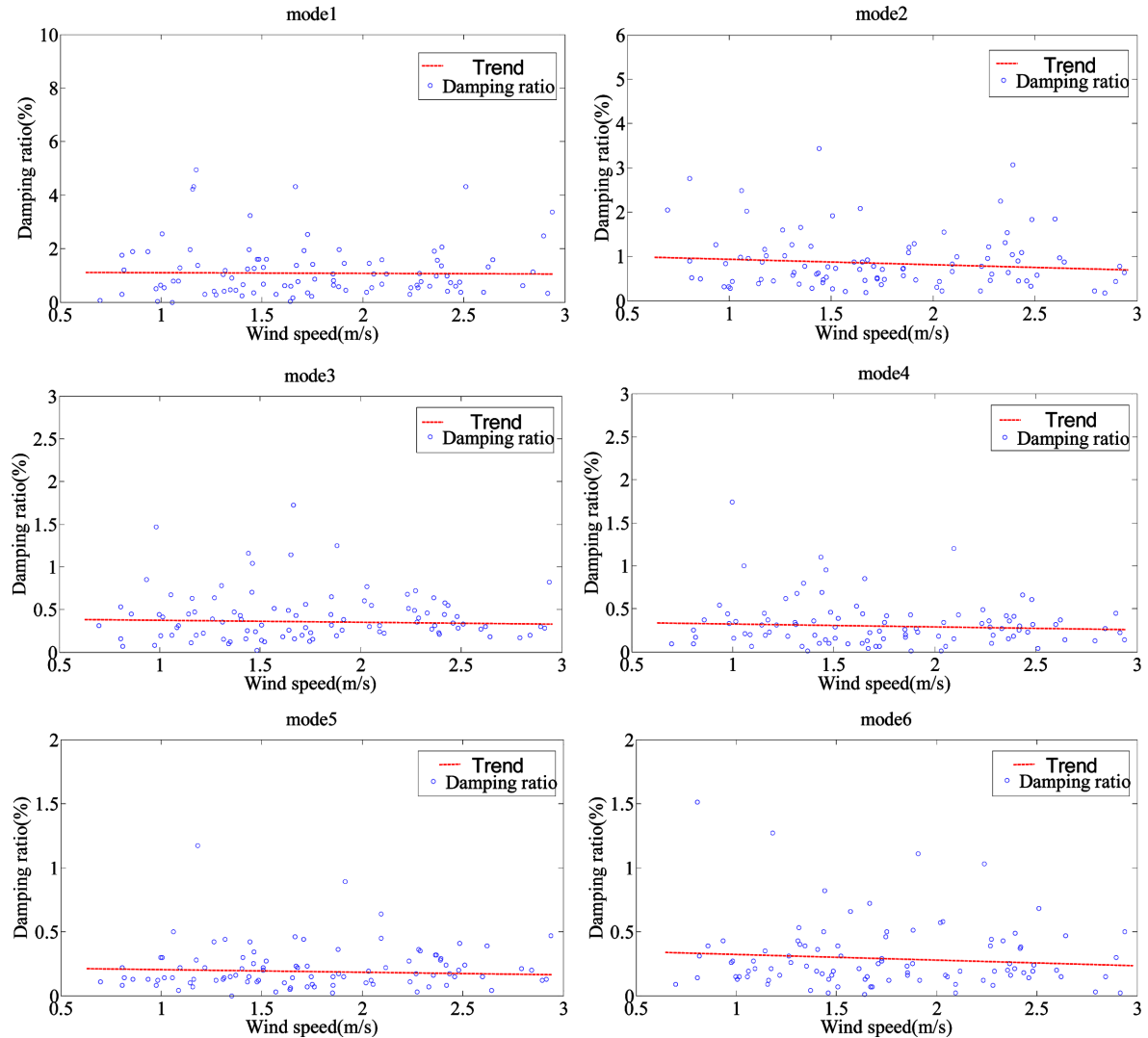


Fig. 13 Variation in damping ratios with wind speed

7. Conclusions

This paper presents the output-only modal identification from a set of monitoring data including acceleration, wind direction, wind speed and ambient temperature, which were recorded during a period of 24 hours on the Canton Tower. Three modal identification methods were applied: (1) EFDD; (2) SSI-DATA; (3) An improved stabilization diagram method based on NExT-ERA. The three methods can successfully identify the first 12 modes, while the improved stabilization diagram method is more robust and automatic than EFDD and SSI-DATA. However, all three methods require human judgment. For instance, in the EFDD method, NFFT, window, and the singular values used to estimate the modal correlation functions have to be defined; in the SSI-DATA method, the dimension of the Hankel matrices and mode order need to be prescribed; in the

improved stabilization diagram method, several critical criteria have to be selected. The selection of these parameters is dependent on the experience of the user. Some suggestions are also given in this study.

Based on the modal identification results, the following conclusions can be made: (1) the natural frequencies identified using different methods are in excellent agreement; (2) the relative difference in the identified damping ratios obtained using different methods is significantly greater than that of the corresponding identified natural frequencies, which can be explained by the well-known fact that modal damping estimation is always crude and not as accurate as modal frequency estimation; (3) the modal damping values identified using different methods are occasionally significantly different, and most of the damping ratios identified using EFDD are greater than those identified using SSI-DATA and NExT-ERA; (4) from the mode shapes in the complex plane, most of the vibration modes identified in this study indicate nonclassical damping, which is due to composite material properties of the tube-in-tube structure of the Canton Tower.

The effect of environmental conditions on the dynamic characteristics of the Canton Tower has been briefly discussed. It is shown that the natural frequencies of the Canton Tower decrease as the ambient temperature increases. The damping ratios data scatter is much larger than that observed in natural frequencies, which does not reach general conclusions. No uniform trend is reflected. This might be due to the low wind speed during the testing period. Further research should be made using the measurement data obtained under high wind speeds.

Acknowledgements

This research was supported by the Foundation of Guangdong Communication Department (2010-02-015). The authors wish to express their sincere thanks to Prof. Y.Q. Ni and Dr. Y. Xia from the Hong Kong Polytechnic University for sharing the field measurement data of the Canton Tower. Appreciation also goes to Dr. Jian Li from UIUC for his valuable suggestions and comments in this research.

References

- Abdel Wahab, M. and De Roeck, G. (1997), "Effect of temperature on dynamic system parameters of a highway bridge", *J. Struct. Eng. - ASCE*, **7**(4), 266-270.
- Allemang, R.J. (1999), *Vibrations: experimental modal analysis*, Course Notes (UC-SDRL-CN-20-263-663/664), Structural Dynamics Research Laboratory, Univ. of Cincinnati, Cincinnati, (<http://www.sdrl.uc.edu/academic-course-info/>).
- Brincker, R., Ventura, C. and Andersen, P. (2001), "Damping estimation by frequency domain decomposition", *Proceedings of the 19th Int. Modal Analysis Conf. (IMAC)*, Kissimmee, Fla., Soc. Experimental Mechanics, Inc., Bethel, Conn.
- Brincker, R., Zhang, L. and Andersen, P. (2000), "Modal identification from ambient responses using frequency domain decomposition", *Proceedings of the 18th Int. Modal Analysis Conf. (IMAC)*, San Antonio, Tex., Soc. Experimental Mechanics, Inc., Bethel, Conn.
- Brown, D.L., Allemang, R.J., Zimmerman, R. and Mergeay, M. (1979), *Parameters Estimation Techniques for Modal Analysis*, Society of Automotive Engineers Technical Paper Series, **88**, 828-846.
- Caicedo, J.M., Dyke, S.J. and Johnson, E.A. (2004), "Natural excitation technique and eigensystem realization algorithm for phase I of the IASC-ASCE benchmark problem: Simulated data", *J. Eng. Mech -ASCE*, **130**(1),

- 49-60.
- Chen, W.H., Lu, Z.R., Lin, W., Chen, S.H., Ni, Y.Q., Xia, Y. and Liao, W.Y. (2011), "Theoretical and experimental modal analysis of the Guangzhou New TV Tower", *J. Eng. Mech -ASCE*, **33**(12), 3628-3646.
- Corrêa, M.R. and Costa, A.C. (1992), *Dynamic Tests of the Bridge over the Arade River*, Cable-stayed bridges of Guadiana and Arade.
- Faravelli, L., Ubertini, F. and Fuggini, C. (2010), "Subspace identification of the Guangzhou New TV Tower", *Proceedings of the 5th World Conference on Structural Control and Monitoring*, Tokyo, Japan.
- He, X., Fraser, M., Conte J.P. and Elgamal, A. (2007), "Investigation of environmental effects on identified modal parameters of the Voigt Bridge", *Proceedings of the 18th Engineering Mechanics Division Conference of the ASCE*, Blacksburg, VA.
- He, X., Moaveni, B., Conte, J.P. and Elgamal, A. (2006), "Comparative study of system identification techniques applied to New Carquinez Bridge", *Proceedings of the 3rd Conf. on Bridge Maintenance, Safety and Management, IABMAS*, Porto, Portugal.
- He, X., Moaveni, B., Conte, J.P., Elgamal, A. and Masri, S.F. (2009), "System identification of Alfred Zampa Memorial Bridge using dynamic field test data", *J. Struct. Eng. - ASCE*, **135**(1), 54-66.
- Hua, X.G., Ni, Y.Q., Ko, J.M. and Wong, K.Y. (2007), "Modeling of temperature-frequency correlation using combined principal component analysis and support vector regression technique", *J. Comput. Civil Eng. - ASCE*, **21**(2), 122-135.
- Ibrahim, S.R. and Mikulcik, E.C. (1977), "A method for the direct identification of vibration parameters from the free response", *Shock Vib.*, **47**(4), 183-198.
- James, G.H., Carne, T.G. and Lauffer, J.P. (1993), *The Natural Excitation Technique for Modal Parameter Extraction from Operating Wind Turbines*, SANDIA REPORT, SAND92-1666. UC-261, Sandia National Laboratories.
- Juang, J.N. and Pappa, R.S. (1985), "An eigensystem realization algorithm for modal parameters identification and model reduction", *J. Guid. Control Dynam.*, **8**(5), 620-627.
- Magalhães, F., Caetano, E. and Cunha, Á.(2007), "Challenges in the application of stochastic modal identification methods to a cable-stayed bridge", *J. Bridge Eng.*, **12**(6), 746-754.
- Nayeri, R.D., Tasbihgoo, F., Wahbeh, M., Caffrey, J., Masri, S., Conte, J. and Elgamal, A. (2009), "Study of time-domain techniques for modal parameter identification of a long suspension bridge with dense sensor arrays", *J. Eng. Mech. -ASCE*, **135**(7), 669-683.
- Ni, Y.Q., Xia, Y., Liao, W.Y. and Ko, J.M. (2009a), "Technology innovation in developing the structural health monitoring system for Guangzhou New TV Tower", *Struct. Control Health Monit.*, **16**(1), 73-98.
- Ni, Y.Q., Zhou, H.F. and Ko, J.M. (2009b), "Generalization capability of neural network models for temperature-frequency correlation using monitoring data", *J. Struct. Eng. - ASCE*, **135**(10), 1290-1300.
- Ni, Y.Q., Xia, Y., Lin, W., Chen, W.H. and Ko, J.M. (2012), "SHM benchmark for high-rise structures: a reduced-order finite element model and field measurement data", *Smart Struct. Syst.*, in this issue.
- Niu, Y., Kraemer, P. and Fritzen, C.P. (2011), "Operational Modal Analysis for the Guangzhou New TV Tower", *Proceedings of the 29th Int. Modal Analysis Conf. (IMAC)*, Jacksonville, Florida, USA.
- Pappa, R.S. (1999), "Independent analysis of the space station node modal test data", *J. Guid. Control Dynam.*, **22**(1), 22-27.
- Pappa, R.S. and Elliott, K.B. (1993), "Consistent-mode indicator for the eigensystem realization algorithm", *J. Guid. Control Dynam.*, **16**(5), 852-858.
- Pappa, R.S., James, G.H. and Zimmerman, D.C. (1998), "Autonomous modal identification of the space shuttle tail rudder", *J. Spacecraft Rockets*, **35**(2), 163-169.
- Peeters, B. and De Roeck, G. (2001), "One-year monitoring of the Z24-Bridge: environmental effects versus damage events", *Earthq. Eng. Struct. D.*, **30**(2), 149-171.
- Prevosto, M. (1982), *Algorithmes d'Identification des Caractéristiques Vibratoires de Structures Mécaniques Complexes*, Ph.D. Thesis, Univ.de Rennes 1, France.
- Sohn, H. (2007), "Effects of environmental and operational variability on structural health monitoring", *Philos. T. R. Soc. A.*, **365**(1851), 539-560.
- Van Overschee, P. and De Moor, B. (1996), *Subspace Identification for Linear Systems: Theory Implementation-Applications*, Kluwer Academic, Norwell, Mass.

- Vold, H., Kundrat, J., Rocklin, G.T. and Russel, R. (1982), *A Multiinput Modal Estimation Algorithm for Minicomputers*, Society of Automotive Engineers Technical Paper Series, **91**, 815-821.
- Xia, Y., Hao, H., Zanardo, G. and Deeks, A. (2006), "Long term vibration monitoring of an RC slab: Temperature and humidity effect", *Eng. Struct.*, **28**(3), 441-452.
- Xia, Y., Xu, Y.L., Wei, Z.L., Zhu, H.P. and Zhou, X.Q. (2011), "Variation of structural vibration characteristics versus non-uniform temperature distribution", *Eng. Struct.*, **33**(1), 146-153.
- Yun, G. J. (2009), *Modal Identification and Damage Detection for Structural Health Monitoring Under Ambient Vibration Environment*, 2009 Structures Congress, Austin, Texas.
- Zhou, H.F., Ni, Y.Q. and Ko, J.M. (2011a), "Eliminating temperature effect in vibration-based structural damage detection", *J. Eng. Mech. - ASCE*, **137**(12), 785-796.
- Zhou, H.F., Ni, Y.Q. and Ko, J.M. (2011b), "Structural damage alarming using auto-associative neural network technique: exploration of environment-tolerant capacity and setup of alarming threshold", *Mech. Syst. Signal Pr.*, **25**(5), 1508-1526.
- Zhou, H.F., Ni, Y.Q., Ko, J.M. and Wong, K.Y. (2008), "Modeling of wind and temperature effects on modal frequencies and analysis of relative strength of effect", *Wind Struct.*, **11**(1), 35-50.